Title: Human voltage-gated Na^+ and K^+ channel properties underlie sustained fast AP signaling

Authors: René Wilbers[1], Verjinia D. Metodieva[1], Sarah Duverdin[1], Djai B. Heyer[1], Anna A. Galakhova[1], Eline J. Mertens[1], Tamara D. Versluis[1], Johannes C. Baayen[2], Sander Idema[2], David P. Noske[2], Niels Verburg[2], Ronald B. Willemse[2], Philip C. de Witt Hamer[2], Maarten H. P. Kole[3,4], Christiaan P.J. de Kock[1], Huibert D. Mansvelder[1]†, Natalia A. Goriounova[1]†

Affiliations:

[1]Department of Integrative Neurophysiology, Center for Neurogenomics and Cognitive Research (CNCR), Vrije Universiteit Amsterdam, Amsterdam Neuroscience; 1081 HV, Amsterdam, the Netherlands.

[2]Department of Neurosurgery, Amsterdam UMC, Vrije Universiteit Amsterdam, Amsterdam Neuroscience, VUmc Cancer Center, Amsterdam Brain Tumor Center; 1081 HV, Amsterdam, the Netherlands.

[3]Department of Axonal Signaling, Netherlands Institute for Neuroscience, Royal Netherlands Academy of Arts and Sciences; 1105 BA Amsterdam, the Netherlands

[4] Cell Biology, Neurobiology and Biophysics, Department of Biology, Faculty of Science, Utrecht University, 3584 CH, Utrecht, The Netherlands

†Corresponding author. Email: n.a.goriounova@vu.nl and h.d.mansvelder@vu.nl

Abstract: Human cortical pyramidal neurons are large, have extensive dendritic trees, and yet have surprisingly fast input-output properties: rapid subthreshold synaptic membrane potential changes are reliably encoded in timing of action potentials (APs). Here, we tested whether biophysical properties of voltage-gated sodium (Na^+) and potassium (K^+) currents in human neurons can explain their fast input-output properties. Human Na^+ and K^+ currents had depolarized voltage-dependence, slower inactivation and exhibited a faster recovery from inactivation than their mouse counterparts. Computational modeling showed that despite lower Na^+ channel densities in human neurons, the biophysical properties of Na^+ channels resulted in higher channel availability and explained fast AP kinetics stability. Finally, human Na^+ channel properties also resulted in a larger dynamic range for encoding of subthreshold membrane potential changes. Thus, biophysical adaptations of voltage-gated Na^+ and K^+ channels enable fast input-output properties of large human pyramidal neurons.

One-Sentence Summary: Biophysical properties of Na^+ and K^+ ion channels enable human neurons to encode fast inputs into output.

Main Text:

Cortical computation relies on neurons to process synaptic inputs and transfer these inputs into action potential (AP) output. Electro-morphological properties of neurons shape their input-output function, determine the speed of transfer and how much of the received synaptic information can be passed on as output to downstream neurons. Human excitatory pyramidal neurons in cortical layers (L) 2 and 3 have large dendritic trees receiving over 30,000 synaptic inputs, twice as many as L2/3 pyramidal neurons in rodent cortex (*1–4*). Encoding activity of large numbers of incoming synaptic inputs would require precise temporal resolution through fast input-output processing properties. This fast encoding can be achieved by precise timing of AP output to incoming synaptic input. (Sub-)millisecond precision of AP (spike) timing carries behaviorally relevant information (*5–7*), and the ability of neurons to respond to inputs with precisely timed spikes is critical to preserve information and distribute it across synaptically coupled neurons (*8*). While the ability of rodent pyramidal neurons to time APs to synaptic input is limited to 200 Hz (*9*, *10*), adult human pyramidal neurons reliably time their APs to subthreshold membrane potential changes of 1000 Hz and above (*11*). Thereby, human L2 and L3 pyramidal neurons have efficient input-output processing properties, with sub-millisecond temporal resolution (*11*). However, mechanisms that enable human pyramidal neurons to reliably encode subthreshold membrane potential changes in AP timing with high temporal precision are poorly understood.

Theoretical studies predict that the speed of AP generation is a critical requirement for fast input-output processing in neuronal networks (*8*, *10*). Fast AP onset kinetics allow neurons to respond readily and reliably to fast changing inputs (*12*), while artificial slow-down of the AP waveform impairs the ability of neurons to encode fast inputs, and slows network processing (*10*). In vivo recordings of single neuron activity in human subjects performing cognitive tasks show that neurons increase their firing to 10-50 Hz from almost silent baseline and maintain high firing rates for minutes (*13–15*). Typically, in such conditions AP kinetics slow down (*16*) and this could impair precise AP timing and reduce efficient encoding. Neurons with slow AP onset mechanisms will not be able to respond to fast synaptic input with an AP, they will 'ignore' fast synaptic inputs. Thus, maintaining fast AP shape could be critical for cognitive function.

We recently showed that human neurons are indeed able to maintain fast and stable AP kinetics during sustained firing and this is relevant for cognitive function (*18*, *19*). Neurons from subjects with higher IQ are able to maintain fast APs, while in subjects with lower IQ the AP rising speed slows down during repeated firing. Furthermore, the encoding ability of single neurons in awake humans has been linked to cognitive task performance (*20*, *21*). Therefore, the ability of human neurons to generate APs with stable shape during repeated firing as well as to encode fast-changing synaptic inputs are inter-related and may play an important role in human cognition. Here we address which biophysical mechanisms underlie fast action potential kinetics and input-output encoding in human neurons. To this end, we recorded APs and underlying voltage-gated sodium (Na^+) and potassium (K^+) currents from pyramidal neurons in supragranular layers (L2 and L3) of human and mouse association cortices. We characterized biophysical properties of voltage-gated Na^+ and K^+ currents underlying action potential generation and used computational modeling to investigate which properties of Na^+ and K^+ channels contribute to human AP kinetics and input-output function.

Results

Stable and fast human AP waveform during repeated firing

During cognitive tasks such as reading, human neurons in the temporal lobe sustain their AP firing for tens of seconds to minutes at frequencies in the range of 10-50 Hz (*13–15*). We first asked whether shape and kinetics of APs in human pyramidal neurons are stable during sustained AP firing, and how this compares to mouse pyramidal neurons. We made whole cell patch-clamp recordings from human and mouse supragranular pyramidal neurons in association cortices and held their membrane potentials to -70 mV. Then we evoked trains of APs with short (3 ms) current pulses at frequencies ranging from 10-70 Hz (Fig. 1A). We observed firing frequency- and time dependent AP broadening, however AP broadening was much more prominent in mouse than human neurons (Fig. 1B-D). Human neurons showed more stable rise and fall speed during repeated firing at all frequencies tested (Fig. 1C-F). Already at a moderate firing frequency of 10 Hz, both rise and fall speed of the 2nd AP showed significantly more slowing down in mouse compared to human neurons (mean rel. rise and fall speed, t-test; $p=0.013$ for rise speed and $p=0.016$ for fall speed, n=34 human cells, n=32 mouse cells), with more pronounced differences at higher frequencies (Fig. 1F). After 200 APs at 70 Hz the effect was most pronounced: median (Q1-Q3, here and further) relative rise speed reduced to 0.56 (0.50-0.67) for mouse neurons (Fig. 1F). In contrast, human neurons sustained their rise speed at a fraction of 0.75 (0.71-0.80) of the initial value, which was significantly higher ($p=6.2*10^{-9}$ Wilcoxon rank sum test). The AP fall speed was also significantly more stable in human neurons (mean±SD here and further, human 0.68±0.11, mouse 0.53±0.12, $p=3.6*10^{-6}$, t-test). The initial speed as well as the stability of the rise and fall speed was similar between neurons from epilepsy and tumor patients (Fig. S1) indicating that stability of AP shape does not depend on disease history.

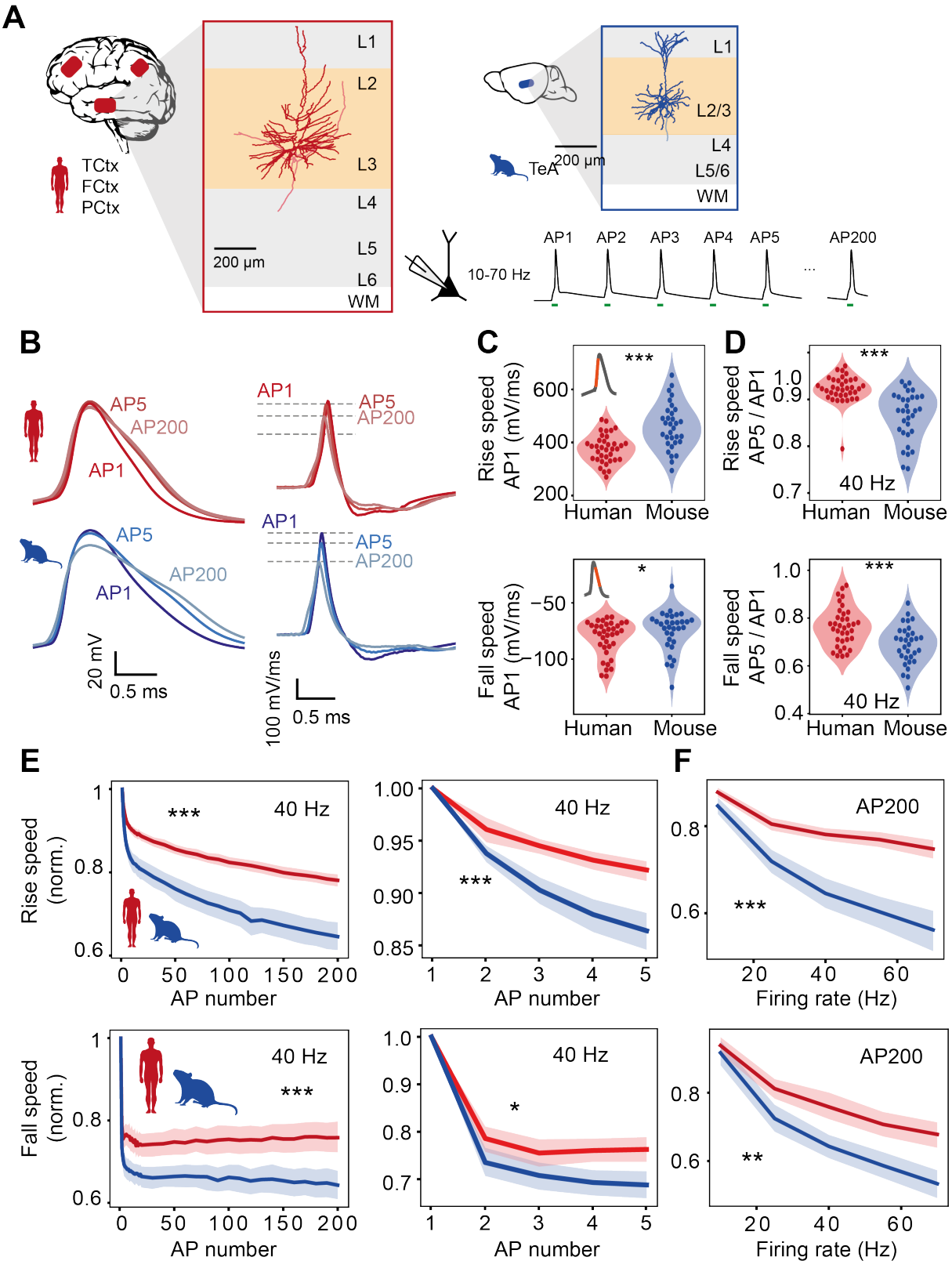

Fig. 1. Stable and fast human AP waveform during repeated firing. (A) Examples of human (red) and mouse (blue) L2/L3 pyramidal neurons: APs at frequencies ranging from 10 to 70 Hz were evoked by short pulses. (B) Examples of human and mouse AP (left) and AP derivative (right) traces illustrating differences in AP stability. (C-F) AP shape stability in human and mouse neurons (human: n=36 cells, mouse: n=32 cells) (C) Absolute rise and

fall speeds of first AP in train. (Rise speed: ***$p<10^{-4}$, unpaired t-test; Fall speed: *p=0.03, Wilcoxon rank sum test). (D) Relative rise and fall speeds of AP5 normalized to AP1 were faster in human neurons. (Rise speed: ***$p<10^{-6}$, Wilcoxon rank sum test; Fall speed: ***$p<10^{-3}$, unpaired t-test) (E) Rise and fall speeds are more stable in human than mouse neurons during repeated APs. Relative rise speed from AP1 to AP200 (left) and AP1 to AP5 (right) during 40 Hz firing showing more slowing of AP kinetics in mouse neurons. (Significance of Species:AP number interaction in linear regression models: Rise speed AP1-200: ***$p<10^{-26}$; Fall speed AP1-200: ***$p<10^{-7}$; Rise speed AP1-5: ***$p<10^{-4}$; Fall speed AP1-5: *p=0.03) (F) Frequency dependence of rise and fall speed stability after 200 APs. (Significance of Species:Frequency interaction effect in linear regression models: ***$p<10^{-9}$, **p=0.001). Shaded areas here and further represent bootstrapped 95% confidence interval of the mean.

Stable Na^+ & K^+ currents during action potentials in human neurons

Since APs mainly arise from a combination of ionic currents through voltage-gated Na^+ and K^+ channels (*22*), we asked whether Na^+ and K^+ currents showed adaptations during repeated firing. We pharmacologically isolated voltage-gated Na^+ and K^+ currents in separate experiments (Fig. S2) and applied AP-train waveform voltage commands to nucleated patches. When a waveform based on a train of 40 Hz was applied, the amplitudes of both Na^+ and K^+ currents significantly decreased from 1st to the 200th AP (Fig 2A). However, Na^+ currents in human patches (n=16) reduced substantially less compared to mouse nucleated patches (n=33), and the difference could be observed already during the first 5 APs (Fig. 2B). Furthermore, K^+ current amplitudes were also more stable with subsequent APs in human neurons (n=14, vs. n=11 mouse neurons), but during the first 5 APs there was no species-specific difference (Fig. 2B). These effects were independent of whether the applied AP command waveform originated from mouse or human neurons (Fig. S3), indicating that intrinsic species differences in Na^+ and K^+ channel properties rather than the shape of the applied AP waveforms is responsible for differences in Na^+ and K^+ current stability.

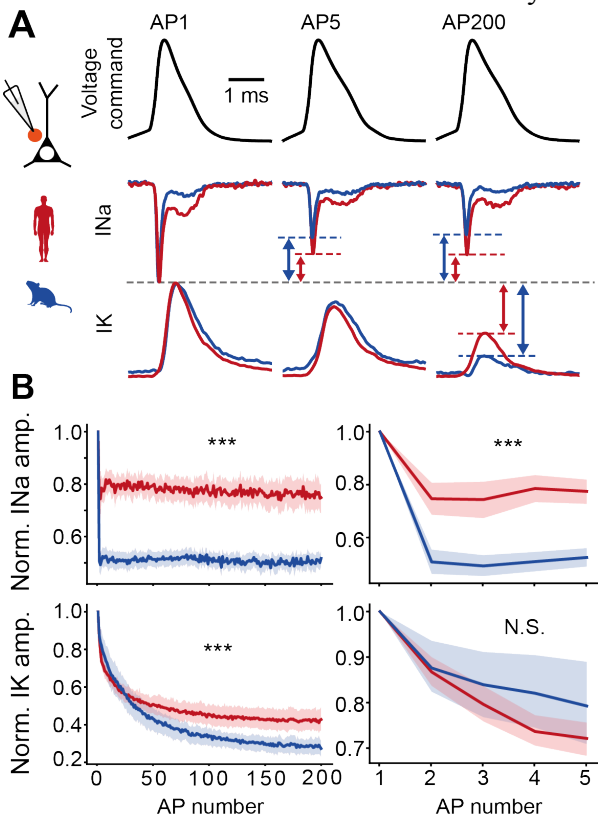

Fig. 2. Stable Na^+ & K^+ currents during human action potentials. (A) Voltage command of AP waveform during repeated firing was applied to nucleated somatic outside-out patches and somatic sodium and potassium currents were recorded (separate experiments). Example currents during AP1, AP5 and AP200 at 40 Hz. Arrows and lines depict the relative difference in current amplitude. (B) Mean normalized Na^+ and K^+ current amplitudes during repeated firing for human and mouse neurons for 200 APs (left) and first 5 APs (right). Asterisks indicate significance of Species:APnumber interaction effect in linear regression model. INa (human: n=16 recordings, mouse: n=33 recordings) amp. 1-200: ***$p<10^{-323}$, amp. 1-5: ***$p<10^{-53}$, IK (human: n=14, mouse: n=11) amp. 1-200: ***$p<10^{-45}$, amp. 1-5: p=0.07.

Voltage-dependence and activation/inactivation kinetics of voltage-gated Na^+ channels

To assess which properties of voltage-gated Na^+ and K^+ currents explain differences in AP shape stability during AP trains, we tested steady-state voltage-dependence as well as activation and inactivation kinetics of human and mouse voltage-gated Na^+ and K^+ currents using square pulses (Figs. 3,5, S4). Strikingly, both steady-state activation and inactivation curves of Na^+ currents were right-shifted by respectively 6 and 9 mV towards more depolarized potentials in human neurons (Fig. 3A,B), indicating that at similar voltages a smaller fraction of Na^+ current was activated and inactivated in human neurons (Table S1, mean±SD $V_{1/2}$ in mV, activation: human= -32.1±4.9, n=19; mouse=-37.9±4.6, n=15, unpaired t-test, p=0.001; inactivation: human= -66.0±7.8, n=18; mouse=-74.8±6.8, n=15, unpaired t-test, p=0.002). At -80 mV, the average Na^+ channel availability measured as relative conductance (G/G_{max}) was 0.81±0.16 for human and 0.63±0.21 for mouse (Fig. 3C). This indicates that compared to mouse, human neurons have a larger fraction of Na^+ channels ready to be activated during the AP upstroke.

The Na^+ current during the AP upstroke is also dependent on the rate of channel inactivation. To characterize the inactivation rate, we fitted single exponentials to inactivating sodium currents at different voltage steps (Fig 3D). At all voltage steps, Na^+ currents in human neurons had slower inactivation time constants than mouse neurons (Fig. 3D). Following an AP, availability of Na^+ channels for the next AP depends on the rate of recovery from inactivation. We fully inactivated channels and used pulses after various recovery voltages and delays to assess time course and voltage-dependence of recovery. Human Na^+ currents had significantly faster recovery time constants at all voltages tested (Fig. 3E). Thus, voltage-gated Na^+ currents in human neurons inactivate more slowly and recover quicker from inactivation than their mouse counterparts, which likely results in less accumulation of inactivated channels after an AP (*17*, *23*) and quicker return to availability to generate the next AP.

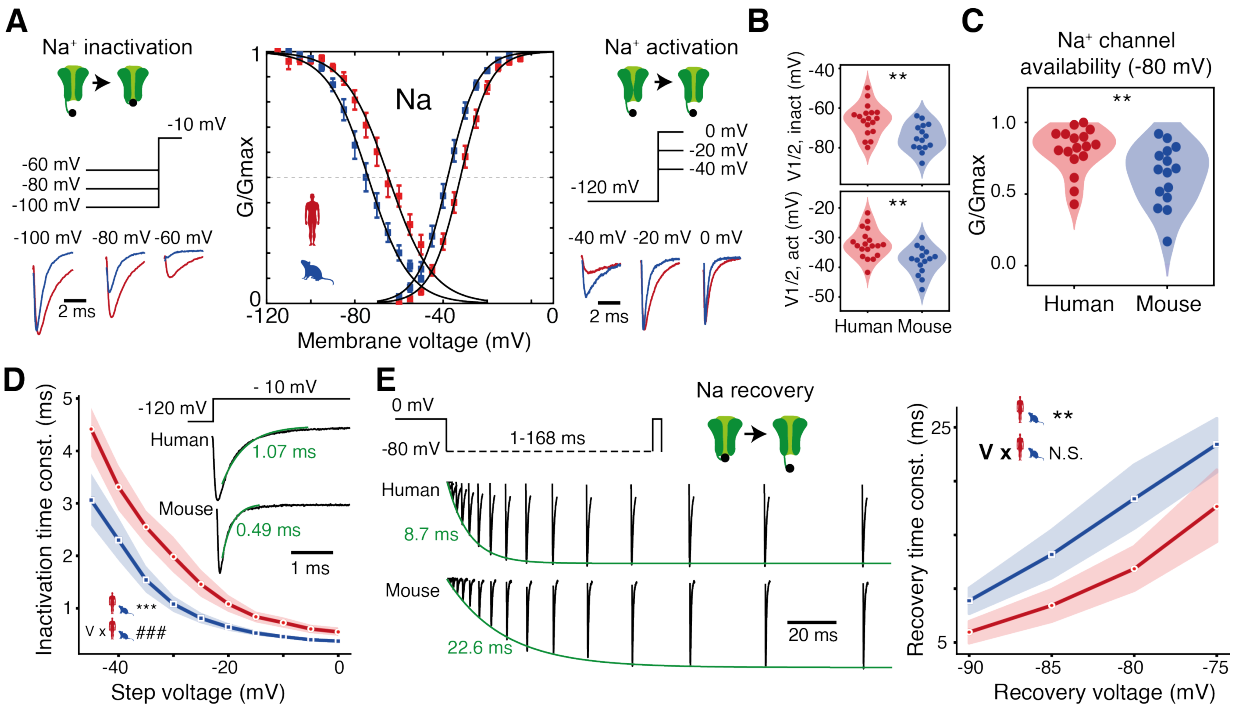

Fig. 3. Voltage-dependence and inactivation kinetics of voltage-gated Na^+ channels. (A) Na^+ currents were evoked following prepulses of incrementing negative voltages (left) and during increasing voltage steps (right) in mouse (blue) and human (red) neurons. Resulting steady-state activation and inactivation conductance curves show a shift to positive voltage for human neurons (middle). Error bars indicate mean ± SEM, black lines are Boltzmann curves fitted to the data. Inactivation: n=18 human recordings and n=15 mouse recordings; Activation: n=19 human recordings and n=15 mouse recordings. (B) Half-activation and half-inactivation voltages are more positive in human neurons (Inact.: **p=0.002, unpaired t-test; Act.: **p=0.001, unpaired t-test). (C) Relative Na^+ conductance availability (G/Gmax) at -80 mV is larger in human neurons (n=17 human recordings and 15 mouse recordings). **p=0.006, Wilcoxon rank sum test. (D) Inactivation time constant was longer in human neurons at all membrane voltages. Inset: example currents with fits and time constants (green)(human: n=19 recordings, mouse: n=15 recordings). ***$p<10^{-21}$ for Species effect and $^{###}p<10^{-7}$ for Voltage:Species interaction effect in polynomial regression model. (E) Example traces of Na^+ current recovery at -80 mV plotted at several inter-pulse durations; exponential fits to corresponding amplitudes are shown in green. Recovery time constant is shorter in human neurons (human: n=19 recordings, mouse: n=15 recordings). ***$p<10^{-7}$ for Species effect and N.S. p=0.17 for Voltage:Species interaction effect in linear regression model.

Increased excess sodium charge during AP firing in human neurons

Our finding that human Na^+ channels inactivate more slowly and to a lesser extent is surprising, as this may come at a cost in terms of energy use. Na^+ channel inactivation halts sodium influx and prevents excess sodium influx during the falling phase of the AP (*17*). Excess sodium influx is energetically unfavorable since ion gradients need to be restored at the cost of ATP (*17*, *24–26*). Given that mouse Na^+ channels show stronger inactivation and recover slowly from inactivation, we hypothesized that mouse neurons show less excess sodium influx during AP firing (Fig. 4). Indeed, in mouse neurons (n=32), the median excess sodium ratio was 2.3 (1.9-2.7), while in human neurons (n=10) it was 3.8 (3.4-4.1, $p<10^{-5}$, Wilcoxon rank sum test). Since it is somewhat counterintuitive that human Na^+ channel properties are less optimized to be energetically favorable, we hypothesized that these properties may contribute to computational aspects of human neurons and further explored this using experiments and modeling.

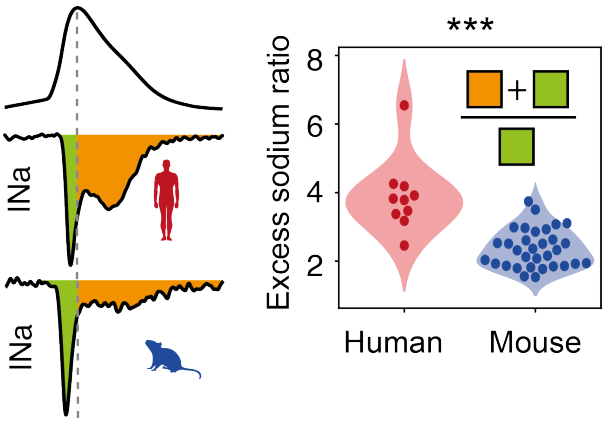

Fig. 4. Increased excess sodium charge during AP firing in human neurons. Left: Sodium current traces during AP voltage waveforms in nucleated patches of human and mouse pyramidal neurons. Green and orange shadings indicate the sodium charge before and after the AP peak. Right: Violin plot of excess sodium ratio in both species (human: n=10 recordings, mouse: n=32 recordings). ***p<10^{-5}, Wilcoxon rank sum test.

Voltage-dependence and activation/inactivation kinetics of voltage-gated K^+ channels

Next, we used square voltage step protocols to nucleated patches and isolated voltage-gated K^+ currents (Methods). The data showed that steady-state activation and inactivation curves (Fig. 5A) were similarly right-shifted towards more depolarized potentials: 5 mV for activation and 12 mV for inactivation (Fig. 5B, Table S1, mean±SD $V_{1/2}$ in mV, activation: human=-3.0±5.9, n=13; mouse=-7.9±6.0, n=29, unpaired t-test, p=0.02; inactivation: human=-52.7±6.0, n=11; mouse=-65.0±5.3, n=26, unpaired t-test, p<10^{-6}). The shift in voltage-dependence of inactivation resulted in a larger average availability of K^+ channels at resting membrane potential of human neurons (human: 0.94±0.05, mouse: 0.86±0.06) (Fig. 5C). Human K^+ currents activated faster than mouse K^+ currents at most tested membrane potentials (Fig. S4B). Inactivation of K^+ currents had a fast- and slow-inactivating component, which were both comparable between species (Fig. 5D). Maximally inactivating K^+ currents and then applying recovery pulses at -80 mV with various delays showed that, although recovery time constants were similar between species, human K^+ currents recovered to a larger proportion of the initial amplitude than their mouse counterparts (Fig 5E), suggesting that part of the mouse K^+ current recovered at much slower rate. Thus, although inactivation and recovery from inactivation kinetics of K^+ currents were similar between species, a large right-shift of steady-state inactivation resulted in higher K^+ channel availability. Moreover, a larger recovery from inactivation is likely to aid repolarization during repeated firing in human neurons.

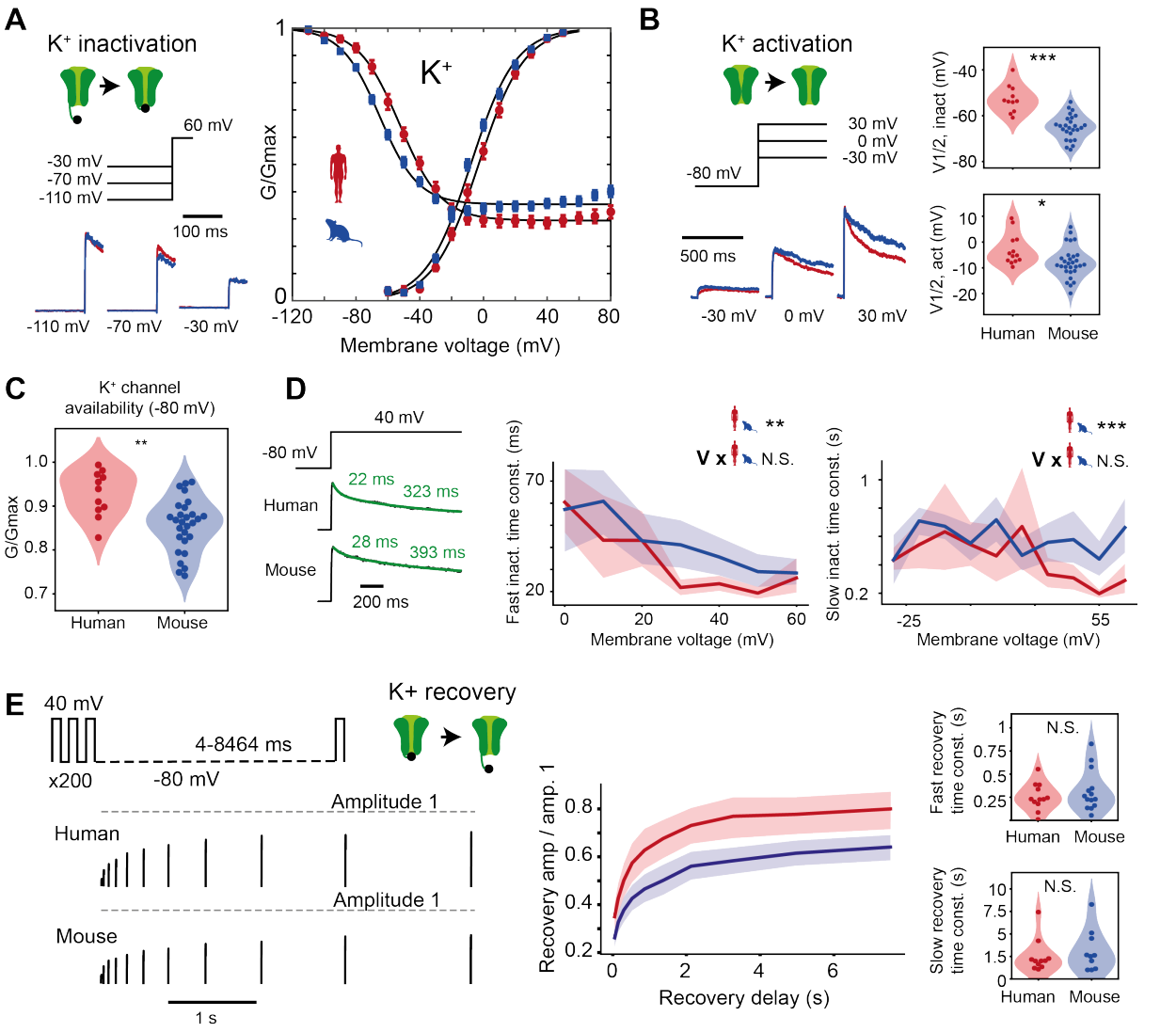

Fig. 5. Voltage-dependence and inactivation kinetics of voltage-gated K^+ channels. (A) K^+ currents were evoked following prepulses of incrementing negative voltages (left) and during increasing voltage steps (right) in mouse (blue) and human (red) neurons. Resulting steady-state activation and inactivation conductance curves show a shift to positive voltage for human neurons (middle). Error bars indicate mean ± SEM, black lines are Boltzmann curves fitted to the data. Inact.: n=11 human recordings and n=28 mouse recordings; Act.: n=13 human recordings and n=29 mouse recordings. (B) Violin plots of half max-(in)activation voltages of individual Boltzmann fits ***$p<10^{-6}$, unpaired t-test; *p=0.02, unpaired t-test). (C) Relative K^+ conductance availability (G/Gmax) at -80 mV is larger in human neurons (n=11 human recordings and 28 mouse recordings). **p=0.001 (D) Left: examples of double exponential fits to inactivating K^+ current traces, yielding fast and slow time constants. Right: Fast and slow K^+ current inactivation time constant versus voltage (n=13 human recordings and 29 mouse recordings). Fast inact.: **p=0.005, Slow inact.: ***p=0.0004, Species effect in linear regression models. (E) Example traces of K^+ current recovery at -80 mV at several inter-pulse durations. Red lines indicate response to first pulse. Right, Top: K^+ current recovery time courses after recovery at -80 mV with several delays (n=12 human recordings and 14 mouse recordings). Right, Bottom: violin plots for fast and slow recovery time constants. N.S.: not significant, Wilcoxon rank sum test.

Human voltage-gated channel properties support stable AP kinetics

Can the differences of voltage-gated Na^+ and K^+ current properties explain the differences in stability of the AP and underlying currents in human and mouse neurons? To test this, we simulated the AP command-voltage clamp experiments with Hodgkin-Huxley (HH) conductance-based models for voltage-gated Na^+ and K^+ channels with properties determined from experimentally observed steady-state curves and transition rates of both species (Fig S5, Table S2). To isolate the role of conductances in AP generation the HH-channel models were implemented in single compartment models containing either human or mouse channels (Fig. 6A). Computational simulations with human ion channels showed more stable voltage-gated Na^+ currents during the first 5 consecutive APs (Fig. 6A,B). Although the model replicated voltage-gated K^+ currents less well, it showed that similar to the experiments, there were no significant differences between human and mouse K^+ currents during the first 5 consecutive APs (Fig. 6C). To examine which specific features of the ion channel cause the differences in Na^+ current stability, we altered mouse Na^+ channel models by stepwise replacing Na^+ channel properties with those of human Na^+ properties and monitored Na^+ current stability. Endowing mouse Na^+ channels with human Na^+ channel activation-related properties did not result in stable Na^+ current properties of human neurons. In contrast, endowing mouse Na^+ channels with inactivation properties of human Na^+ channels produced stability of Na^+ currents during repeated AP firing replicating the experimentally recorded properties in human neurons (Fig. 6D). Both steady-state voltage-dependence (G/Gmax) as well as time constants of inactivation and recovery contribute to this effect. This suggests that the slow Na^+ channel inactivation and fast recovery from inactivation are critical for Na^+ current stability in human neurons.

Next, we asked whether voltage-gated Na^+ and K^+ channel properties predicted from the current recordings support AP shape stability. To this end, we simulated AP firing by HH-based single compartment models with varying fractions of human and mouse voltage-gated Na^+ and K^+ channels, with constant total channel densities. Both Na^+ and K^+ channel properties of human neurons result in more stable APs. Gradually replacing mouse Na^+ and K^+ channels with their human counterparts increased the speed of both the rise and falling phase of APs (Fig. 6E-F). The amplitude of APs also increased with increasing fractions of human Na^+ and K^+ channels relative to mouse channels. Experimentally, however, amplitudes of the first AP did not differ between species (Fig. 1). One explanation for this discrepancy between model and experiment could be that the peak conductance densities are distinct between species. Simulating membrane conductance densities at different fractions of human and mouse voltage-gated Na^+ and K^+ channels showed that with larger fractions of human channel properties lower conductance densities were required (Fig. 6G). We next measured experimentally the conductance densities of pharmacologically isolated Na^+ or K^+ currents in nucleated patches from human and mouse neurons. Remarkably, both Na^+ and K^+ conductance densities were lower in human neurons compared to mouse neurons (Fig. 6H, Table S3, mean ± SEM $pS*\mu m^{-2}$: human Na^+ 5.9±0.8; n=17 recordings, mouse Na^+ 13.4±1.2; n=15 recordings, human K^+ 31.2±4.2; n=13 recordings, mouse K^+ 43.5±2.8; n=24 recordings). This experimental data confirms the differences in current densities obtained in the model fits (6G). Next, we updated the HH models with the obtained fitted channel densities in the models for each specific combination of channel fractions. The simulations revealed that the shape of the first AP was now similar between mouse and human conductance-based models (Fig. 6I), as observed experimentally (Fig. 1C). Rise and fall speeds as well as amplitudes of APs were more stable in models based on increasingly human Na^+ channel properties. Human K^+ channel properties did not improve AP stability during the first five APs. (Fig. 6I-J), but did so after 200 APs (Fig S6). Thus, improved stability of AP shape in

human neurons can be explained by properties of their voltage-gated Na^+ and K^+ channels, despite lower channel densities.

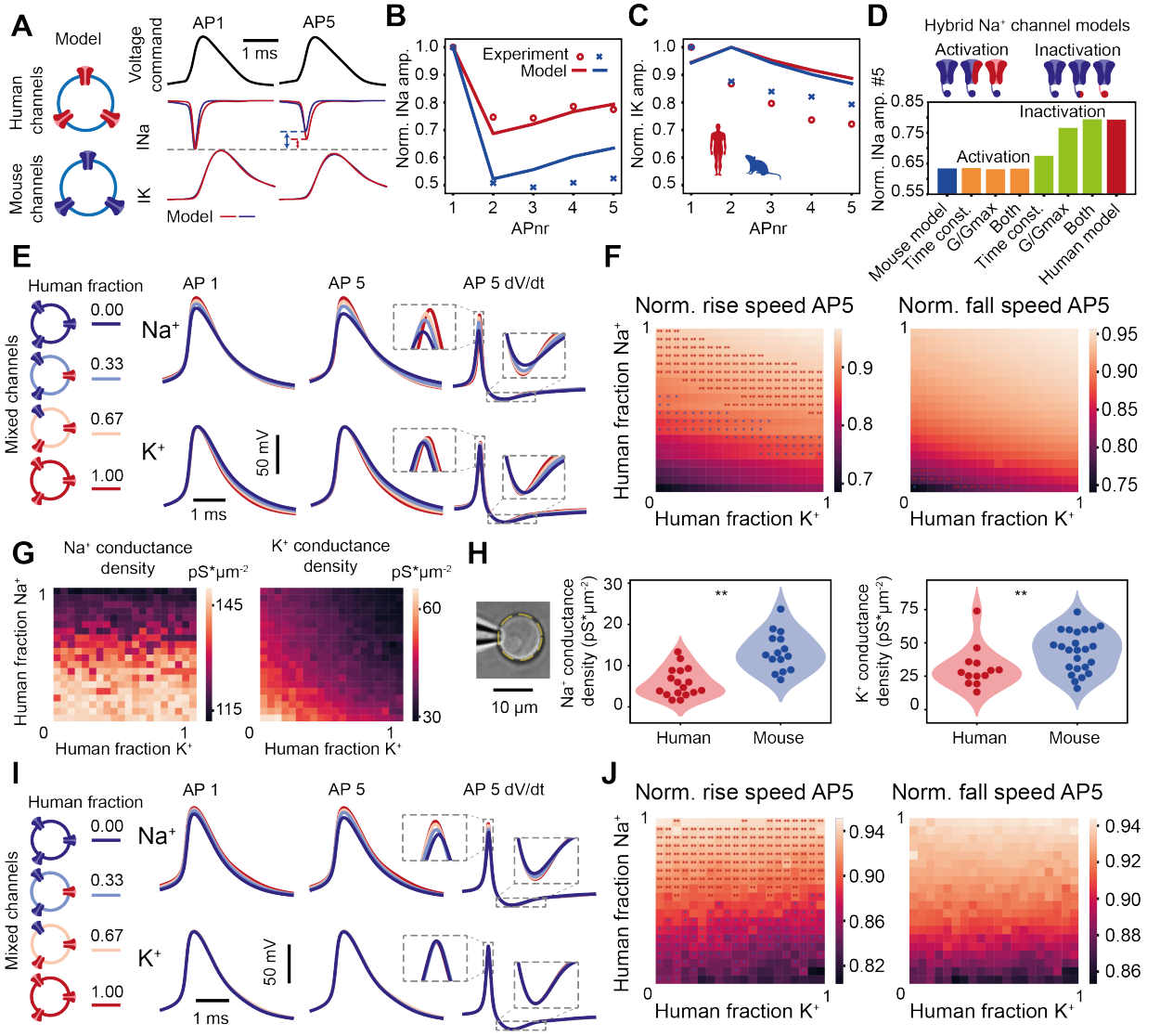

Fig. 6. Human voltage-gated channel properties support stable AP kinetics. (A) HH models of human and mouse somatic Na^+ and K^+ channels based on fits to experimental data. Example traces of simulated Na^+ and K^+ currents during AP command voltage-clamp experiment. (B,C) Relative amplitudes of simulated and experimentally recorded Na^+ and K^+ currents. (D) Na^+ current stability in different hybrid mouse-human Na^+ channel models: stepwise changing different activation and inactivation properties of Na^+ channels from mouse to human results in Na^+ current stability (current amplitude at fifth AP / current amplitude at first AP). (E) Active AP firing model with variable fractions of human and mouse Na^+ and K^+ channels. Example traces of first AP, fifth AP and derivative of the fifth AP for various human proportions for Na^+ (top) and K^+ (bottom) channel simulations. (F) Human/mouse channel fractions affect rise (left) and fall (right) speeds of the fifth AP relative to the first AP. Asterisks indicate results near (±0.02) experimental means from Fig.1D. (G) Na^+ and K^+ conductance densities at different human/mouse channel fractions. (H) Experimentally recorded Na^+ and K^+ conductance densities in nucleated patches of human and mouse neurons (Na^+ human: n=17 recordings, Na^+ mouse: n=15 recordings, K^+ human: n=13 recordings, K^+ mouse: n=24 recordings) (I), (J) Active AP firing HH-model as in (E). (F) but with matched best-fit channel densities from (G).

Human ion channel properties and Na^+ channel availability support fast input-output conversion

Ongoing synaptic transmission results in dynamic sub-threshold dendritic membrane potential changes that may or may not be encoded into AP output (*27*). The extent to which the fine temporal structure of membrane potential changes can be encoded, i.e. how large the bandwidth is of the neuronal transfer function, depends on the stability of AP rise speed properties (*10*). Could the identified biophysical features of human Na^+ and K^+ channels underlie the unique encoding properties in human pyramidal neurons (*11*)? To assess the contribution of human and mouse voltage-gated Na^+ and K^+ channel properties to the bandwidth of the input-output function of human and mouse neurons, we applied sub-threshold membrane potential changes with varying frequencies to the HH-conductance models with human and mouse Na^+ and K^+ channel properties. Model neurons were injected with a DC depolarization to generate APs at frequencies of ~12.5 Hz. On top of the DC component, model neurons received subthreshold sinusoid input currents of increasing frequencies and a Gaussian noise component (Fig. 7A). For each AP, we determined its timing relative to the phase of the injected subthreshold sinusoidal waveform. To quantify phase-locking of AP timing to the sinusoidal input, we generated peri-stimulus time histograms (PSTH) for different sinusoidal input frequencies and calculated the amplitude relative to its mean (M/R) of the best-fit sinusoid to this histogram (Fig. 7B). At similar firing rates in simulations with human and mouse channel properties, M/R was larger, e.g AP phase-locking was stronger, in models with human channel properties across all frequencies (Fig 7C). When the DC input current level was decreased in the model with mouse channel properties, the firing rate dropped to ~9 Hz and M/R recovered in the lower frequency range. The cutoff frequency was defined as the input frequency at which the phase-locking (M/R) drops below 0.4. Strikingly, this cutoff frequency was 73 Hz in the model based on human channels, nearly 2-fold higher than 38-42 Hz we obtained in models with mouse channels (Fig 7C).

Since Na^+ current properties were largely responsible for stable AP shapes in human neurons (see above), we asked whether species differences in Na^+ channel inactivation properties would affect the bandwidth of AP phase-locking to input frequencies. To answer this, we quantified for each individual AP the average fraction of sodium channel availability for activation (*h*, see Methods) in the 2 ms preceding AP onset, as well as the AP timing relative to the input sinusoid (Fig. 7D,E). The fraction of available sodium channels (*h*) just before the AP was substantially higher in model simulations with human Na^+ channel inactivation properties (Fig. 7E, median human $h = 0.55$; median mouse $h = 0.45$). For both human and mouse Na^+ channel property models, APs that had above median Na^+ channel availability (*h*) values just before onset were more strictly timed to the input sinusoid than APs with low *h* values (Fig. 7E). Thus, larger sodium channel availability improves phase-locking of AP timing. To test whether sodium channel availability also affected the bandwidth of phase-locking, we varied *h* values in HH-model simulations by varying the relative proportions of voltage-gated channels with human and mouse properties. Increasing the fraction of channels with human properties increased the cutoff frequency of AP phase-locking to sinusoidal inputs to higher frequencies (Fig. 7F), thereby increasing the bandwidth of the input-output transfer function. Thus, properties of human voltage-gated Na^+ and K^+ channels support AP shape stability and contribute to improved input-output function of human neurons.

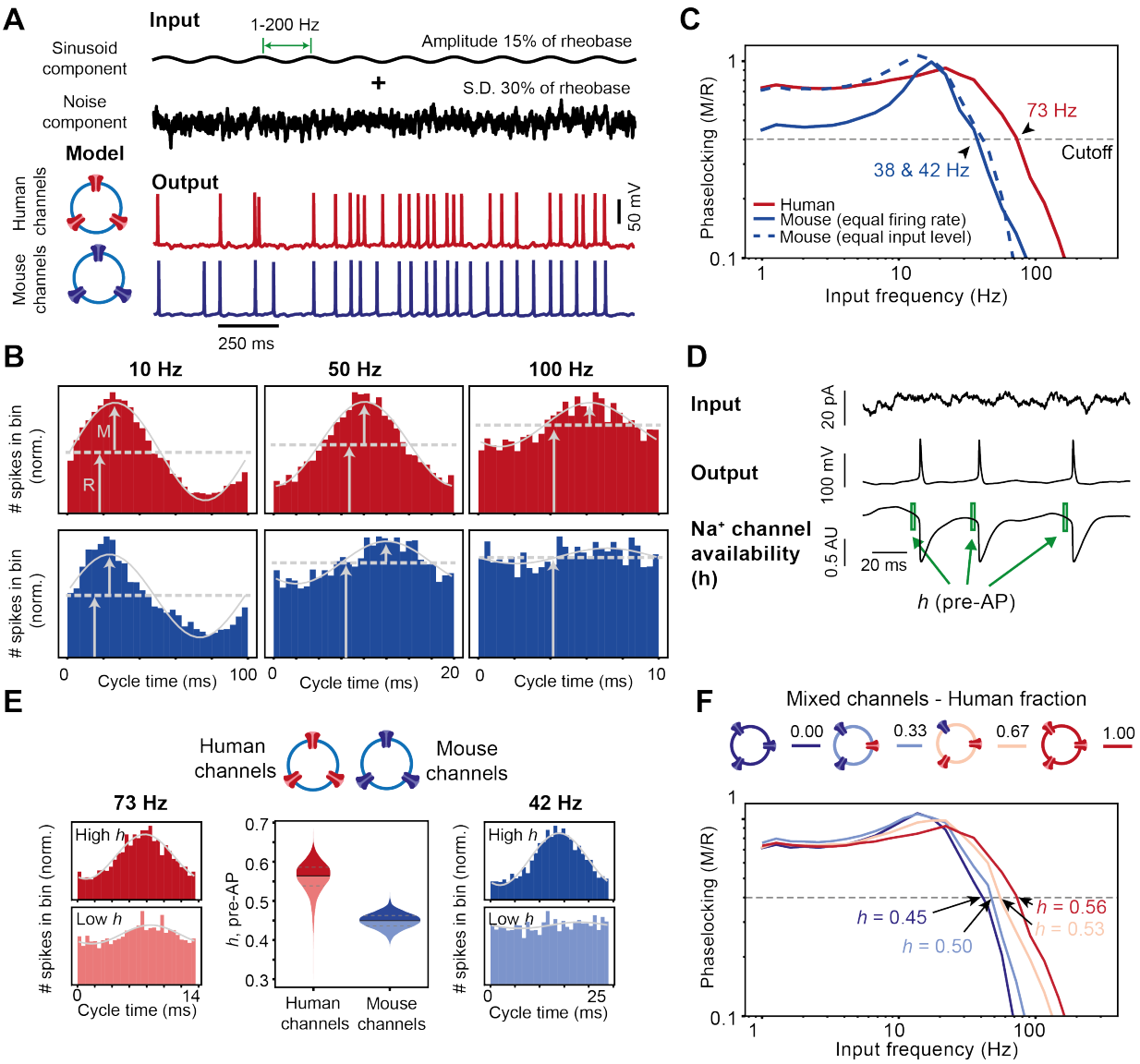

Fig. 7. Human ion channel properties and Na$^+$ channel availability support fast input-output conversion. (A) Input current components of AP firing HH-model simulations (top traces, DC component not depicted) and example output traces (bottom traces, input frequency 5 Hz). (B) PSTHs of APs timed within the sinusoid cycle. Grey lines: sinusoidal fit to histogram; Black lines: Input sinusoidal current. Arrows indicate mean R and amplitude M of fitted sinusoid, which determine degree of phase-locking (M/R). (C) Phase-locking as function of input frequencies for human and mouse Na$^+$ channel models. Arrows indicate cutoff frequencies. Hatched blue line: mouse Na$^+$ channel simulations with same input current as human Na$^+$ channel simulations. Solid blue line: mouse Na$^+$ channel simulations with input current adjusted to AP rate ~13 Hz (D) Example traces of Na$^+$ channel availability (h) resulting from a sinusoid input with added noise. Pre-AP Na$^+$ channel availability is calculated as mean of h during 0.8-.2.8 ms before the AP peak (green boxes). (E) Relative timing of APs to sinusoids at cutoff frequency observed in human (left, input frequency 76 Hz) and mouse (right, input frequency 44 Hz) HH-model simulations with below and above median pre-AP h values. Middle panel: Distributions of pre-AP h values of all APs in human and mouse channel-based HH-model simulation. (F) HH-model simulations with different fractions of human and mouse voltage-gated channel properties.

Discussion

In this study, we identified biophysical mechanisms that underlie fast and stable input-output properties of human pyramidal neurons during repeated AP firing. Both Na^+ and K^+ currents had right-shifted steady-state voltage-dependence compared to mouse pyramidal neurons. Voltage-gated K^+ currents in human neurons activated faster and showed more recovery from inactivation. Voltage-gated Na^+ currents showed slower, and reduced inactivation and faster recovery from inactivation. With model simulations we showed that this resulted in larger functional availability of Na^+ channels to maintain fast AP onset. Increased availability of Na^+ channels enable human neurons to time APs to faster subthreshold membrane potential changes, providing these neurons with a larger bandwidth input-output transfer function. These findings provide mechanistic insights into how Na^+ and K^+ channels give rise to fast input-output conversion in human pyramidal neurons, the computational building block of the brain.

The rate of AP onset is an important determinant of the ability of neurons to time their AP to inputs (*10*, *12*, *28*). Properties of voltage-gated sodium channels that favor larger availability of activatable sodium channels are therefore ideally placed to support fast input-output processing. However, voltage-gated sodium and potassium channels are not the only factors. Several recent studies have identified human neuron properties that contribute to fast input-output processing. Firstly, large dendritic structure of human neurons increases dendritic conductance load and improves AP onset kinetics and phase-locking to high input frequencies (*28*), which was later also confirmed for realistic human morphologies (*18*). Secondly, human pyramidal neurons unlike rodents express HCN channels in both human pyramidal neurons (*29*) and fast-spiking interneurons (*30*) and these channels help speed up the time course at which synaptic inputs arrive at the soma. Lastly, the duration of distal dendritic spikes is dramatically shorter in human neurons when compared to other mammals (*31*).

Sub-millisecond AP timing is not unique in nature. Spike timing with a temporal resolution smaller than the time scales of sensory and motor signals, even at sub-millisecond levels, encode significant amounts of visual information in the fly visual system (*6*). Subcortical neurons in the auditory system neurons can phase lock their firing to auditory frequencies up to ~1 to 2 kHz (*32–34*). However, it is surprising that the large pyramidal neurons in L3 of the human temporal association cortex can time APs with sub-millisecond resolution. It is likely that in evolution several cellular and biophysical adaptations have occurred in human cortical neurons that work in concert to support a fast input-output processing that reliably converts synaptic inputs into timed AP output.

Although there is strong supporting evidence that both AP stability and phase-locking are associated with human cognitive performance (*18–20*), it is currently not known how exactly these cellular features contribute to improved network function. However, a recent study found that AP speed and dendritic size of human neurons are related to individual differences in functional network integration (*35*). Furthermore, the faster time-course of inputs together with the ability to reliably convert them to outputs must result in a faster total signaling speed, which would add up cumulatively during network computations. Indeed, the reaction time of individuals is negatively correlated to their intelligence (*36*), suggesting that processing speed plays an important role in cognition. A recent study found that a network model with human-like fast synaptic recovery speeds performed more accurately than a model with rodent like slow synaptic recovery (*37*), indicating that fast and frequent computations might contribute to improved network function. The fast recovery from inactivation we observed in human sodium channels leads to larger sodium channel availability, which will further speed up processing in neuronal networks, since it facilitates rapid AP induction in response to synaptic depolarization.

The ability of human neurons to reliably encode highly dynamic subthreshold membrane potential changes with increased reliability in spike timing may allow human neuronal networks to encode information more sparsely (*38*). Although sparse coding has not been compared between humans and rodents, a recent study found that neighboring neurons in human cortex fire less synchronously than in monkey (*39*), suggesting extraordinary sparse coding in human cortex. Indeed, concept neurons in human medial temporal lobe typically respond sparsely, to about 0.5% of concepts (*40*). This would not only increase the number of concepts that can be encoded by a neuronal network (*41*), but would also make the encoding more energy efficient per concept. Thereby there could be a trade-off between energy efficiency at the single neuron level versus energy efficiency at the neuronal network and concept level. We found that reduced Na^+ channel inactivation and faster recovery from inactivation in human neurons go together with a larger excess influx of sodium during AP firing. While slow or incomplete inactivation of voltage-gated sodium channels during an action potential leads to increased sodium influx and is energetically wasteful (*17*, *23*, *24*, *26*), we here found that these Na^+ channel properties enable fast input-output processing and improved AP timing to synaptic input. This suggests that while these inactivation dynamics improve information encoding they come at a cost of metabolic efficiency. Recent evidence has shown that such a tradeoff exists, since mouse neurons reduce their coding precision to save energy during lack of caloric intake (*42*). At the neuronal network level, coding precision that improves bandwidth and content may allow networks to encode with fewer neurons, and thereby overall spend less energy.

Our results show that Na^+ and K^+ currents in human neurons have substantially different properties than mouse neurons. Candidate molecular mechanism explaining these differences could be differential expression of Na^+ and K^+ channel subunits in mouse versus human neurons. Proteomic studies have shown that in hippocampal synapses several alpha and beta subunits of sodium channels are differentially expressed between rodents and primates (*43*). Genes encoding voltage-gated Na^+ and K^+ channels are highly conserved (*44*). However, functionality of the pore-forming alpha subunits can be modulated in several manners, such as auxiliary beta subunits, phosphorylation (*45*, *46*), cytoskeleton anchoring and splicing factors (*47*). Although the molecular basis for the adaptations of Na^+ and K^+ channel to support fast input-output processing in human is currently unknown, the HH-conductance-based channel models we used to fit human Na^+ and K^+ currents do provide clues pointing to voltage-sensitivity and rate of inactivation properties.

Despite an increased availability of activatable channels, we did observe a reduced density of Na^+ and K^+ conductance in human neurons. This is in line with recent work which found that human cortical neurons have exceptionally low K^+ and HCN conductance compared to 9 other mammalian species (*31*). Without biophysical adaptation of sodium and potassium channels, a reduced density of sodium and potassium channels would have dramatic consequences for neuronal excitability: an elevated threshold for AP firing and slower input-output processing (*8*). However, our findings on biophysical adaptations can explain why human neurons are not silent and have fast and stable input-output processing: right-shifted inactivation curves to more depolarized membrane potential values, reduced inactivation and recovery from inactivation provide a larger proportion of Na^+ and K^+ channels available for activation at resting membrane potential. Our simulations show that these properties compensate the reduced conductance density in human neurons, and are vital to understand human cortical function from its neurons up (*48*, *49*).

References and Notes

1. J. J. Hutsler, D. G. Lee, K. K. Porter, Comparative analysis of cortical layering and supragranular layer enlargement in rodent carnivore and primate species. *Brain Res.* **1052**, 71–81 (2005).
2. H. Mohan, M. B. Verhoog, K. K. Doreswamy, G. Eyal, R. Aardse, B. N. Lodder, N. A. Goriounova, B. Asamoah, A. B. C. B. Brakspear, C. Groot, S. Van Der Sluis, G. Testa-silva, J. Obermayer, Z. S. R. M. Boudewijns, R. T. Narayanan, J. C. Baayen, I. Segev, H. D. Mansvelder, C. P. J. De Kock, Dendritic and Axonal Architecture of Individual Pyramidal Neurons across Layers of Adult Human Neocortex. *Cereb. Cortex*, 1–15 (2015).
3. G. N. Elston, R. Benavides-Piccione, J. DeFelipe, The pyramidal cell in cognition: a comparative study in human and monkey. *J. Neurosci.* **21**, 1–5 (2001).
4. J. DeFelipe, L. Alonso-Nanclares, J. I. Arellano, Microstructure of the neocortex: Comparative aspects. *J. Neurocytol.* **31**, 299–316 (2002).
5. Y. Zuo, H. Safaai, G. Notaro, A. Mazzoni, S. Panzeri, M. E. Diamond, Complementary contributions of spike timing and spike rate to perceptual decisions in rat S1 and S2 cortex. *Curr. Biol.* **25**, 357–363 (2015).
6. I. Nemenman, G. D. Lewen, W. Bialek, R. R. D. R. Van Steveninck, Neural coding of natural stimuli: Information at sub-millisecond resolution. *PLoS Comput. Biol.* **4** (2008), doi:10.1371/journal.pcbi.1000025.
7. P. Tiesinga, J. M. Fellous, T. J. Sejnowski, Regulation of spike timing in visual cortical circuits. *Nat. Rev. Neurosci.* **9**, 97–107 (2008).
8. M. Volgushev, Cortical Specializations Underlying Fast Computations. *Neurosci.* **22**, 145–164 (2016).
9. H. Köndgen, C. Geisler, S. Fusi, X. J. Wang, H. R. Lüscher, M. Giugliano, The dynamical response properties of neocortical neurons to temporally modulated noisy inputs in vitro. *Cereb. Cortex*. **18**, 2086–2097 (2008).
10. V. Ilin, A. Malyshev, F. Wolf, M. Volgushev, Fast computations in cortical ensembles require rapid initiation of action potentials. *J. Neurosci.* **33**, 2281–2292 (2013).
11. G. Testa-Silva, M. B. Verhoog, D. Linaro, C. P. J. de Kock, J. C. Baayen, R. M. Meredith, C. I. De Zeeuw, M. Giugliano, H. D. Mansvelder, High Bandwidth Synaptic Communication and Frequency Tracking in Human Neocortex. *PLOS Biol.* **12**, e1002007 (2014).
12. N. Fourcaud-Trocmé, D. Hansel, C. Van Vreeswijk, N. Brunel, How Spike Generation Mechanisms Determine the Neuronal Response to Fluctuating Inputs. *J. Neurosci.* **23**, 11628–11640 (2003).
13. R. Quian Quiroga, A. Kraskov, C. Koch, I. Fried, Explicit Encoding of Multimodal Percepts by Single Neurons in the Human Brain. *Curr. Biol.* **19**, 1308–1313 (2009).
14. R. Quian Quiroga, L. Reddy, G. Kreiman, C. Koch, I. Fried, Invariant visual representation by single neurons in the human brain. *Nature*. **435**, 1102–1107 (2005).
15. M. M. Haglund, G. A. Ojemann, T. W. Schwartz, E. Lettich, Neuronal activity in human

lateral temporal cortex during serial retrieval from short-term memory. *J. Neurosci.* **14**, 1507–1515 (1994).

16. B. P. Bean, The action potential in mammalian central neurons. *Nat. Rev. Neurosci.* **8** (2007), pp. 451–465.
17. B. C. Carter, B. P. Bean, Sodium Entry during Action Potentials of Mammalian Neurons: Incomplete Inactivation and Reduced Metabolic Efficiency in Fast-Spiking Neurons. *Neuron*. **64**, 898–909 (2009).
18. N. A. Goriounova, D. B. Heyer, R. Wilbers, M. B. Verhoog, M. Giugliano, C. Verbist, J. Obermayer, A. Kerkhofs, H. Smeding, M. Verberne, S. Idema, J. C. Baayen, A. W. Pieneman, C. P. de Kock, M. Klein, H. D. Mansvelder, Large and fast human pyramidal neurons associate with intelligence. *Elife*. **7**, 1–21 (2018).
19. D. B. Heyer, R. Wilbers, A. A. Galakhova, E. Hartsema, S. Braak, S. Hunt, M. B. Verhoog, M. L. Muijtjens, E. J. Mertens, S. Idema, J. C. Baayen, P. D. W. Hamer, M. Klein, M. McGraw, E. S. Lein, C. P. J. De Kock, H. D. Mansvelder, N. A. Goriounova, P. de Witt Hamer, M. Klein, M. McGraw, E. S. Lein, C. P. J. de Kock, H. D. Mansvelder, N. A. Goriounova, Verbal and General IQ Associate with Supragranular Layer Thickness and Cell Properties of the Left Temporal Cortex. *Cereb. Cortex* (2021), doi:10.1093/cercor/bhab330.
20. U. Rutishauser, I. B. Ross, A. N. Mamelak, E. M. Schuman, Human memory strength is predicted by theta-frequency phase-locking of single neurons. *Nature*. **464**, 903–907 (2010).
21. L. Reddy, M. W. Self, B. Zoefel, M. Poncet, J. K. Possel, J. C. Peters, J. C. Baayen, S. Idema, R. VanRullen, P. R. Roelfsema, Theta-phase dependent neuronal coding during sequence learning in human single neurons. *Nat. Commun.* **12**, 1–9 (2021).
22. A. L. Hodgkin, A. F. Huxley, Currents carried by sodium and potassium ions through the membrane of the giant axon of Loligo. *J. Physiol.* **116**, 449–472 (1952).
23. B. C. Carter, B. P. Bean, Incomplete inactivation and rapid recovery of voltage-dependent sodium channels during high-frequency firing in cerebellar Purkinje neurons. *J. Neurophysiol.* **105**, 860–871 (2011).
24. S. Hallermann, C. P. J. De Kock, G. J. Stuart, M. H. P. Kole, State and location dependence of action potential metabolic cost in cortical pyramidal neurons. *Nat. Neurosci.* **15**, 1007–1014 (2012).
25. H. Hu, F. C. Roth, D. Vandael, P. Jonas, Complementary Tuning of Na+ and K+ Channel Gating Underlies Fast and Energy-Efficient Action Potentials in GABAergic Interneuron Axons. *Neuron*. **98**, 156-165.e6 (2018).
26. H. Alle, A. Roth, J. R. P. Geiger, Energy-efficient action potentials in hippocampal mossy fibers. *Science (80-.).* **325**, 1405–1408 (2009).
27. J. F. A. Poulet, C. C. H. Petersen, Internal brain state regulates membrane potential synchrony in barrel cortex of behaving mice. *Nature*. **454**, 881–885 (2008).
28. G. Eyal, H. D. Mansvelder, C. P. J. de Kock, I. Segev, Dendrites impact the encoding capabilities of the axon. *J. Neurosci.* **34**, 8063–8071 (2014).

29. B. E. Kalmbach, A. Buchin, B. Long, C. A. Anastassiou, E. S. Lein, J. T. Ting, B. E. Kalmbach, A. Buchin, B. Long, J. Close, A. Nandi, J. A. Miller, h-Channels Contribute to Divergent Intrinsic Membrane Properties of Supragranular Pyramidal Neurons in Human versus Mouse Cerebral Cortex Article h-Channels Contribute to Divergent Intrinsic Membrane Properties of Supragranular Pyramidal Neurons in Human . *Neuron*. **100**, 1194-1208.e5 (2018).

30. V. Szegedi, E. Bakos, S. Furdan, P. Barzo, G. Tamas, K. Lamsa, *bioRxiv*, in press, doi:10.1101/2021.06.09.447671.

31. L. Beaulieu-Laroche, N. J. Brown, M. Hansen, E. H. S. Toloza, J. Sharma, Z. M. Williams, M. P. Frosch, G. R. Cosgrove, S. S. Cash, M. T. Harnett, Allometric rules for mammalian cortical layer 5 neuron biophysics. *Nature*. **600**, 274–278 (2021).

32. A. Bieser, P. Müller-Preuss, Auditory responsive cortex in the squirrel monkey: Neural responses to amplitude-modulated sounds. *Exp. Brain Res.* **108**, 273–284 (1996).

33. P. X. Joris, C. E. Schreiner, A. Rees, Neural Processing of Amplitude-Modulated Sounds. *Physiol. Rev.* **84**, 541–577 (2004).

34. C. E. Schreiner, J. V. Urbas, Representation of amplitude modulation in the auditory cortex of the cat. II. Comparison between cortical fields. *Hear. Res.* **32**, 49–63 (1988).

35. L. Douw, I. A. Nissen, S. M. D. D. Fitzsimmons, F. A. N. Santos, A. Hillebrand, E. C. W. van Straaten, C. J. Stam, P. C. De Witt Hamer, J. C. Baayen, M. Klein, J. C. Reijneveld, D. B. Heyer, M. B. Verhoog, R. Wilbers, S. Hunt, H. D. Mansvelder, J. J. G. Geurts, C. P. J. de Kock, N. A. Goriounova, Cellular Substrates of Functional Network Integration and Memory in Temporal Lobe Epilepsy. *Cereb. Cortex* (2021), doi:10.1093/cercor/bhab349.

36. G. Der, I. J. Deary, The relationship between intelligence and reaction time varies with age: Results from three representative narrow-age age cohorts at 30, 50 and 69 years. *Intelligence*. **64**, 89–97 (2017).

37. Q. Zhang, Y. Zeng, T. Zhang, T. Yang, Comparison Between Human and Rodent Neurons for Persistent Activity Performance: A Biologically Plausible Computational Investigation. *Front. Syst. Neurosci.* **15**, 98 (2021).

38. B. A. Olshausen, D. J. Field, Sparse coding of sensory inputs. *Curr. Opin. Neurobiol.* **14**, 481–487 (2004).

39. R. Pryluk, Y. Kfir, R. Pryluk, Y. Kfir, H. Gelbard-sagiv, I. Fried, R. Paz, A Tradeoff in the Neural Code across Regions and Species. *Cell*, 1–13 (2019).

40. S. Waydo, A. Kraskov, R. Quian Quiroga, I. Fried, C. Koch, Sparse representation in the human medial temporal lobe. *J. Neurosci.* **26**, 10232–10234 (2006).

41. G. Eyal, M. B. Verhoog, G. Testa-Silva, Y. Deitcher, R. B. Piccione, J. DeFelipe, C. P. J. de Kock, H. D. Mansvelder, I. Segev, Human cortical pyramidal neurons: From spines to spikes via models. *Front. Cell. Neurosci.* **12**, 1–24 (2018).

42. Z. Padamsey, D. Katsanevaki, N. Dupuy, N. L. Rochefort, Neocortex saves energy by reducing coding precision during food scarcity. *Neuron*, 1–17 (2021).

43. F. Koopmans, N. J. Pandya, S. K. Franke, I. H. C. M. H. Phillippens, I. Paliukhovich, K. W. Li, A. B. Smit, Comparative Hippocampal Synaptic Proteomes of Rodents and

Primates: Differences in Neuroplasticity-Related Proteins . *Front. Mol. Neurosci.* . **11** (2018), (available at https://www.frontiersin.org/article/10.3389/fnmol.2018.00364).

44. M. S. Martin, B. Tang, N. Ta, A. Escayg, Characterization of 5′ untranslated regions of the voltage-gated sodium channels SCN1A, SCN2A, and SCN3A and identification of cis-conserved noncoding sequences. *Genomics*. **90**, 225–235 (2007).

45. M. Li, J. W. West, Y. Lai, T. Scheuer, W. A. Catterall, Functional modulation of brain sodium channels by cAMP-dependent phosphorylation. *Neuron*. **8**, 1151–1159 (1992).

46. T. Scheuer, Regulation of sodium channel activity by phosphorylation. *Semin. Cell Dev. Biol.* **22**, 160–165 (2011).

47. D. A. Buchner, M. Trudeau, M. H. Meisler, SCNM1, a putative RNA splicing factor that modifies disease severity in mice. *Science (80-.).* **301**, 967–969 (2003).

48. S. Grillner, N. Ip, C. Koch, W. Koroshetz, H. Okano, M. Polachek, M. M. Poo, T. J. Sejnowski, Worldwide initiatives to advance brain research. *Nat. Neurosci.* **19**, 1118–1122 (2016).

49. C. Eliasmith, O. Trujillo, The use and abuse of large-scale brain models. *Curr. Opin. Neurobiol.* **25**, 1–6 (2014).

50. J. L. Teeters, K. Godfrey, R. Young, C. Dang, C. Friedsam, B. Wark, H. Asari, S. Peron, N. Li, A. Peyrache, G. Denisov, J. H. Siegle, S. R. Olsen, C. Martin, M. Chun, S. Tripathy, T. J. Blanche, K. Harris, G. Buzsáki, C. Koch, M. Meister, K. Svoboda, F. T. Sommer, Neurodata Without Borders: Creating a Common Data Format for Neurophysiology. *Neuron*. **88**, 629–634 (2015).

51. M. L. Hines, N. T. Carnevale, The NEURON Simulation Environment. *Neural Comput.* **9**, 1179–1209 (1997).

52. Z. F. Mainen, J. Joerges, J. R. Huguenard, T. J. Sejnowski, A model of spike initiation in neocortical pyramidal neurons. *Neuron*. **15**, 1427–1439 (1995).

53. M. H. P. Kole, S. Hallermann, G. J. Stuart, Single Ih channels in pyramidal neuron dendrites: Properties, distribution, and impact on action potential output. *J. Neurosci.* **26**, 1677–1687 (2006).

54. N. Hansen, A. Ostermeier, Completely Derandomized Self-Adaptation in Evolution Strategies. *Evol. Comput.* **9**, 159–195 (2001).

55. F. A. Fortin, F. M. De Rainville, M. A. Gardner, M. Parizeau, C. Gagńe, DEAP: Evolutionary algorithms made easy. *J. Mach. Learn. Res.* **13**, 2171–2175 (2012).

Acknowledgements

We would like to thank Dr. Tim Heistek and Ing. Hans Lodder for excellent technical assistance.

Funding

European Union's Horizon 2020 Framework Programme for Research and Innovation, specific grant agreement no. 945539 (Human Brain Project SGA3)

ERANET programme iPS&BRAIN

Netherlands Organization for Scientific Research (NWO) Gravitation program BRAINSCAPES: A Roadmap from Neurogenetics to Neurobiology (NWO: 024.004.012)
National Institute of Mental Health (NIMH) award U01MH114812.
Netherlands Organization for Scientific Research (NWO) VI.Vidi.213.014 grant

Author contributions

Conceptualization, R.W., N.A.G., H.D.M. and C.P.J.d.K.

Methodology, R.W., N.A.G. and M.H.P.K.

Software, R.W.

Investigation, R.W., V.M., S.D., D.B.H., A.A.G., E.J.M. and T.D.V.

Formal analysis, R.W.

Funding acquisition, H.D.M.

Resources, J.C.B., S.I., D.P.N., N.V., R.B.W., P.C.d.w.H.

Supervision, N.A.G. R.W., H.D.M. and C.P.J.d.K.

Visualization, R.W. and N.A.G.

Writing – original draft, R.W.

Writing – review & editing, R.W., N.A.G., H.D.M., C.P.J.d.K., M.H.P.K.

Competing interests: The authors declare that they have no competing interests

Data and materials availability: All data will be publicly available at (link will be inserted in final version). All model files and model code are available at https://senselab.med.yale.edu/ModelDB/... (link will be updated in final version). All code to reproduce figures is available at https://github.org/... (link will be updated in final version).

Supplementary Materials

Materials and Methods

Figs. S1 to S6

Tables S1 to S3

References (*50-55*)